IOP Publishing Nanotechnology

Nanotechnology **31** (2020) 465403 (13pp) https://doi.org/10.1088/1361-6528/abae30

Tuning the thermal conductivity of nanoparticle suspensions by electric field

Zi-Tong Zhang[1,3], **Ruo-Yu Dong**[1,2,3], **De-shan Qiao**[1] **and Bing-Yang Cao**[1]

[1] Key Laboratory for Thermal Science and Power Engineering of Ministry of Education, Department of Engineering Mechanics, Tsinghua University, Beijing 100084, People's Republic of China
[2] Center for Soft and Living Matter, Institute for Basic Science (IBS), Ulsan 44919, Republic of Korea

E-mail: caoby@tsinghua.edu.cn

Received 28 June 2020, revised 29 July 2020
Accepted for publication 11 August 2020
Published 26 August 2020

Abstract

Active thermal management is essential for the operation of modern technologies like electronic circuits and spacecraft systems to deal with the complex control and conversion of thermal energy. One basic requirement for the materials is its tunable and reversible thermal properties. Here, we try to provide a systematic investigation of the thermal smart materials composed of low-dimensional solid particles suspended in liquid media, whose structures and properties can be tuned by external field. A two-step theoretical model, which takes into account the effects from particle aggregation and orientational variation, was proposed and obtained reasonable agreement with both literature and our own experimental results. Graphene nanosheets/Mg-Al layered double hydroxides (GNS/LDH) were fabricated and their silicone oil suspension shows reversible thermal conductivity switching under DC electric field due to the formation/break-up of chain-like structures with a maximum switching ratio around 1.35×. This study reveals the underlying mechanism of thermal conductivity enhancement in nanoparticle suspensions, and provides a preliminary example to design and fabricate responsive thermal materials for the next generation technologies.

Keywords: thermal conductivity, reversible tuning, electric field, graphene nanosheets

(Some figures may appear in colour only in the online journal)

Nomenclature

E	Electrical field strength (V/mm)
k_f	Thermal conductivity of base fluid (W/(m · K))
k_p	Thermal conductivity of particles (W/(m · K))
k_{eff}	Thermal conductivity of the suspension (W/(m · K))
$k_{cluster}$	Thermal conductivity of particle aggregates (W/(m · K))
k^*_{eff}	Thermal conductivity tensor of the suspension
k_{ij}	Thermal conductivity tensor of anisotropic particles
L	Geometrical factor
p	Aspect ratio of particle aggregates
p'	Aspect ratio of particle

Greek symbols

θ	Particle orientation
ϕ	Volume fraction of particles in suspension
ϕ_{int}	Volume fraction of particles in the aggregates
$\phi_{cluster}$	Volume fraction of aggregates in suspension

1. Introduction

The demand of effective management of heat transfer is increasing in various up-to-date application scenarios including electronic devices [1], spacecraft components [2] and power generation systems [3]. Rising on top of traditional passive strategies to manipulate thermal transport, active techniques have gained much attention in recent years to cope with the prominent temperature and energy fluctuations under complex conditions. Thermal switches [4], thermal rectifiers

[3] These authors contributed equally to this work.

[5, 6] and thermal transistors [7] are some of the examples that people have invented with dynamic and controllable characteristics of thermal transports. New functionalities are thus endowed by these new thermal 'smart' devices analogous to their electronic counterparts [8]. Among the design principles of these advanced components, active and reversible tuning of thermal conductivities of materials, namely thermal smart materials, lies at the core, requiring a switching between the on (high)/off (low) states or a continuous variation of the conductivity values.

Several mechanisms and experimental realizations have been reported regarding the reversible manipulation of thermal conductivities. The thermal regulation might result from the solid-liquid phase transition of graphite/hexadecane suspensions [9] or rotational structural phase transition of crystalline polyethylene nanofibers [10]; alignment of liquid crystal networks under magnetic field [11] or alignment of azobenzene polymers under light triggering [12]; reconfigured nanoscale ferroelastic domain structure and wall density of lead zirconate titanate films under electric field [13]; reversible delithiation of $LiCoO_2$ cathode materials under electrochemical tuning [14]; and variation of topological networks of the tandem repeat proteins by desiccation- hydration cycles [15]. The above strategies realized a thermal switching ratio ranging from $\sim$1.1$\times$ to $\sim$10$\times$ spanning distinctively different systems.

Another big possibility of active thermal regulation comes from low-dimensional materials, like graphene flakes and carbon nanotubes, suspended in liquid solutions. Under electric field [16], magnetic field [17] or shear flow [18], these non-spherical particles prefer to align along the field direction and form chain-like structures, leading to anisotropic electric conductivity [16] or shear thinning behavior [19]. Inspired by these studies, we hypothesize that the thermal conductivity of the suspension should also be tunable under these external fields as properly aligning these low-dimensional materials in solid-state nanocomposites can lead to enhanced thermal properties along the alignment direction [20, 21]. In liquid solutions, without external fields, these particles distribute randomly in terms of both spatial positions and orientations. The dynamics of these particles are governed by translational and rotational Brownian diffusion at equilibrium [22], while the application of some external field will restrict the random motion and make particles to orient along a specific direction [23, 24]. Taking electric field as an example, the particles are polarized to form dipoles, which can be further coupled with the field to generate a torque to orient the particles along the electric direction, make the particles to migrate to the electrodes due to dielectrophoresis and form end-to-end contacts and chains due to Coulomb forces [25]. Reversible control of this process by turning on and off the electric field can also be realized by using good dispersive particles, like graphene oxide (GO), and the resulting electro-rheological (ER) fluids possess reversible rheological properties [26, 27]. To the best of our knowledge, little research was conducted along this direction to reversibly tune the thermal conductivities of particle suspensions, except for the work in [28] where the magnetic field was applied to the magnetic graphite suspensions and achieved $\sim$3$\times$ thermal switching ratio. However, the equipment to generate magnetic field is relatively complex and cumbersome. Comparing to magnetic field, the generation of DC/AC electric field is considered simpler with faster response and lower energy consumption, but the exploration using electric field to realize materials with tunable thermal properties is still lacking.

To account for the experimental observation, appropriate theoretical models are required to link the gap between microstructural changes and the variation of thermal conductivities in the suspension. Maxwell [29] first proposed the thermal conductivity of mixtures based on effective medium theory, assuming the system is composed of continuum medium and embedded spherical particles. Later on, various studies added the effects like non-sphericity [30], inter-particle interactions [31], particle Brownian motion [32] and solid-liquid interface [33] to modify the Maxwell model. The above-mentioned formation of chain-like structures under electric field implies that particle aggregation and orientation are another two non-trivial effects. Although Prasher *et al* [34] and Nan *et al* [35] separately included one of these two effects into their models and achieved certain success to match with the experimental results, a comprehensive model that considers both effects and deals with the reversible tuning of thermal conductivities is needed at the current stage.

In this work, we propose a two-step theoretical model to predict the thermal conductivity of particle suspensions, taking into account both the effects of particle aggregation and orientational variation. The newly derived model was tested against literature experimental results in terms of the above two effects separately and the obtained good agreements fully confirm the validity of the model, which was further used to fit our own experiments later. Experimentally, we fabricated graphene nanosheets/Mg-Al layered double hydroxides (GNS/LDH) and dispersed them in silicone oil. Using electric field, we recorded the formation dynamics of chain-like aggregates spanning the two electrodes and its structural reversibility. A thermal switching ratio around 1.35$\times$ along the chain direction was obtained. This work might guide the future preparation of thermal responsive materials by revealing the respective contributions from particle properties, shapes and arrangements on the effective system thermal conductivity and the rough calculation at the optimal condition provides a maximum thermal swithing ratio, which requires further experimental testing. The GNS/LDH suspension surves as one of the preliminary experimental attempts and the proposed fabrication and characterization strategies might be of relevance to future experimental designs.

2. Methods

2.1. Two-step model

Previous studies have shown that the micro/nanoparticles in suspensions will arrange along the electric field direction and form chain structures, leading to structural anisotropy and enhanced thermal conductivity along the chain direction compared to the case of random particle distributions. The orientation and agglomeration of particles are thus the two key

factors to affect the tunable thermal conductivity of suspensions. Based on this, we propose a two-step model taking into account of both these two factors. The traditional theoretical model of Maxwell [29] is applicable to solid particles in liquid media with small volume fraction of particles and ignores the interaction between them. The Maxwell model states that

$$\frac{k_{eff}}{k_f} = \frac{k_p + 2k_f + 2\phi(k_p - k_f)}{k_p + 2k_f - \phi(k_p - k_f)} \tag{1}$$

where k_{eff}, k_f, k_p are the thermal conductivities of the suspension, base fluid and particles, respectively and ϕ is the particle volume fraction. The Maxwell model is only suitable for spherical isotropic particles and low particle volume fraction. Considering the enhancement of thermal conductivity caused by particle anisotropy, the second-order tensor should be introduced to describe the thermal conductivity instead of a scalar value:

$$k^*_{\text{eff}} = \begin{bmatrix} k_{11} & 0 & 0 \\ 0 & k_{22} & 0 \\ 0 & 0 & k_{33} \end{bmatrix} \tag{2}$$

where k^*_{eff} is the thermal conductivity tensor of the suspension, k_{33} is the effective thermal conductivity parallel to the electric field direction, and k_{22} and k_{11} are the effective thermal conductivity perpendicular to it.

As shown in figure 1, under electric field, the solid particles in the suspension arrange in an end-to-end manner and form elongated chains. These chains can be regarded as the aggregates of solid particles with an aspect ratio p. In the first step of our model, we calculate the thermal conductivity of the particle aggregates, based on the Bruggeman effective medium theory [31]:

$$\phi_{int}\left(\frac{k_p - k_{cluster}}{k_p + 2k_{cluster}}\right) + (1 - \phi_{int})\left(\frac{k_f - k_{cluster}}{k_f + 2k_{cluster}}\right) = 0 \tag{3}$$

Here ϕ_{int} and $\phi_{cluster}$ is the volume fraction of the solid particles in the aggregates and the volume fraction of the aggregates in suspension, respectively, and we have the relation $\phi = \phi_{cluster} \cdot \phi_{int}$ due to number conservation of the particles. Taking into account of the non-sphericity of the low-dimensional materials, the thermal conductivity of the aggregates $k_{ij}^{cluster}$ can be written as

$$k_{11}^{cluster} = k_{22}^{cluster} = k_f \frac{k_{11} + k_f + \phi_{int}(k_{11} - k_f)}{k_{11} + k_f - \phi_{int}(k_{11} - k_f)} \tag{4}$$

$$k_{33}^{cluster} = (1 - \phi_{int})k_f + \phi_{int}k_{33}. \tag{5}$$

where k_{ij} is the second-order tensor of thermal conductivity defined in equation (2) for anisotropic particles.

In the second step of our model, we calculate the thermal conductivity of the system considering the contribution of the particle orientations, based on effective medium theory of Nan *et al* [35]:

$$k^*_{ij} = \delta_{ij}k_f + k_f \frac{\phi_{cluster}A_{ij}}{\delta_{ij} - \phi_{cluster}B_{ij}} \tag{6}$$

Here k^*_{ij} is the thermal conductivity of the suspension, and A_{ij} and B_{ij} are expressed as

$$A_{ij} = \left\langle \frac{k_{ij}^{cluster} - k_f}{k_f + L_{ii}\left(k_{ij}^{cluster} - k_f\right)} \right\rangle,$$
$$B_{ij} = \left\langle \frac{L_{ii}\left(k_{ij}^{cluster} - k_f\right)}{k_f + L_{ii}\left(k_{ij}^{cluster} - k_f\right)} \right\rangle. \tag{7}$$

where $\langle \ldots \rangle$ denotes orientational averaging, and L_{ii} is the geometrical factor depending on p [35, 36].

$$L_{11} = L_{22} = \frac{p^2}{2(p^2 - 1)} - \frac{p}{2(p^2 - 1)^{\frac{3}{2}}}\cosh^{-1}p \tag{8}$$

$$L_{33} = 1 - 2L_{11} \tag{9}$$

If we assume that the suspension is isotropic on the plane perpendicular to the electric field, we get $k_{11}^{cluster} = k_{22}^{cluster}$, $L_{11} = L_{22}, k_{11} = k_{22}$. Equation (6) can be rewritten as

$$k^*_{11} = k_f + k_f \frac{\phi_{cluster}A_{11}}{1 - \phi_{cluster}B_{11}}. \tag{10}$$

$$k^*_{33} = k_f + k_f \frac{\phi_{cluster}A_{33}}{1 - \phi_{cluster}B_{33}}. \tag{11}$$

And we have

$$A_{11} = \frac{k_{11}^{cluster} - k_f}{k_f + L_{11}\left(k_{11}^{cluster} - k_f\right)} \frac{1 + \cos^2\theta}{2} + \frac{k_{33}^{cluster} - k_f}{k_f + L_{33}\left(k_{33}^{cluster} - k_f\right)} \frac{1 - \cos^2\theta}{2} \tag{12}$$

$$A_{33} = \frac{k_{11}^{cluster} - k_f}{k_f + L_{11}\left(k_{11}^{cluster} - k_f\right)}\left[1 - \cos^2\theta\right] + \frac{k_{33}^{cluster} - k_f}{k_f + L_{33}\left(k_{33}^{cluster} - k_f\right)}\cos^2\theta \tag{13}$$

where $\cos^2\theta = \int^{\rho}(\theta)\cos^2\theta \sin\theta\, d\theta / \int^{\rho}(\theta)\sin\theta\, d\theta$, $\rho(\theta)$ is the particle orientation distribution function. Following the above procedure, the newly proposed model successively calculates the contributions from particle agglomerations and anisotropic particle orientations to the effective system thermal conductivity, and are thus termed 'two step' theoretical model.

2.2. Preparation of GNS/LDH-silicon oil suspensions

The preparation of GNS/LDH-silicon oil suspension is based on a one-pot hydrothermal method [37]. First, GO was synthesized from natural graphite plates (Sinopharm Chemical Reagent Co. Ltd. of China) by an improved Hummers method [38, 39]. The detailed procedures are as follows: 360 ml concentrated sulfuric acid was mixed with 40 ml phosphoric acid thoroughly. Then 18 g potassium permanganate and 3 g natural graphite flakes were slowly added to the solution. The mixture was stirred at 55 °C for 12 h and placed in ice bath with the addition of 30% (3 ml) hydrogen peroxide. The solution was further centrifuged and the supernatant was decanted

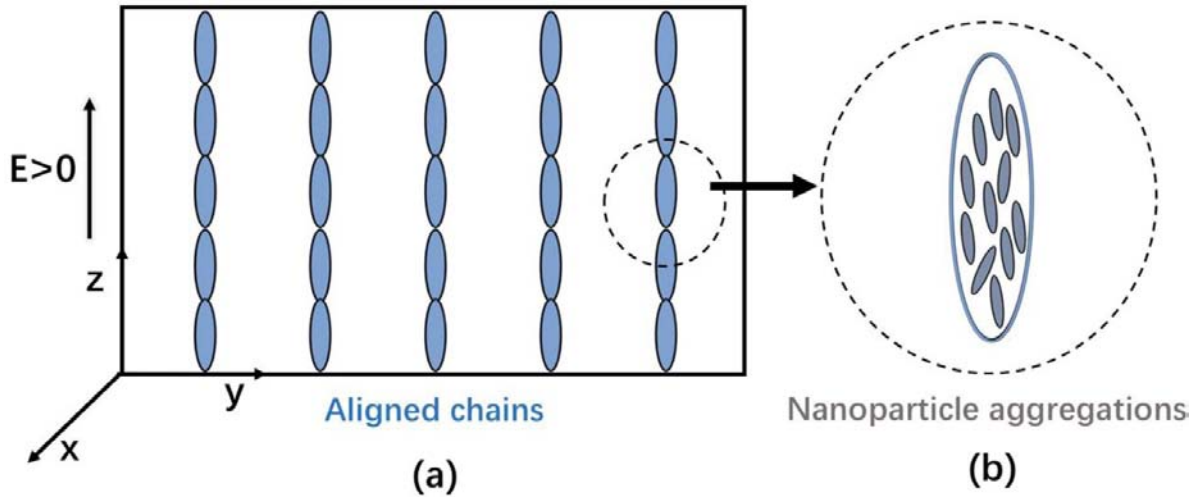

Figure 1. The schematic diagram showing the arrangement of solid particles in suspension under external field. (a) The chain structures are composed of particle aggregates along the direction of external field. (b) The enlarged view of one particle aggregates.

away. The remaining solid materials were rinsed with deionized water until the pH turned neutral. Ultrasonication and dilution was then performed to obtain 5 mg ml^{-1} GO colloidal dispersion.

To make GNS/LDH composites, we mixed 2 g GO dispersion with 80 ml solution containing 5.120 g $Mg(NO_3) \cdot 6H_2O$, 3.750 g $Al(NO_3)_3 \cdot 9H_2O$ and 3.640 g hexamethylenetetramine (Sinopharm Chemical Reagent Co. Ltd. of China) under vigorous stirring. The solution was ultrasonicated for 1 h, transferred into a stainless autoclave and heated for 12 h at 140°C. The precipitate was then separated, rinsed and dried in vacuum to obtain the GNS/Mg-Al layered double-hydroxide (GNS/LDH) composites. The thus-obtained mixture had a GNS weight fraction around 1%. Finally, we dispersed the GNS/LDH composites into the silicon oil and the resulting suspension was ready for further tests.

2.3. Characterization and measurements

The morphology of the as-prepared GNS/LDH composites was observed by scanning electron microscopy (SEM, JSM-6700 F) at an accelerated voltage of 20 kV. To quantify the thermal properties of the GNS/LDH suspension, *in situ* thermal measurement of the sample at the presence of electric field is required. Considering that the sample is in liquid phase with structural anisotropy, we selected laser flash method [40] by using LFA 467 HyperFlash (Netzsch) as it can perform one-dimensional (1D) and non-contact measurements. We designed an integrated sample cell to hold the liquid sample and arrange the electric conducting pathway, as shown in figure 2. The electric field direction (and the formed chain direction) is parallel to the direction of thermal measurement. The cell has an upper and a lower aluminum covers connected with electric wires to ensure a uniform electric field, which was generated by a DC power supply (Keysight, N5752A), across the liquid sample. The insulating inner layers and outer shells could prevent short circuit due to possible inappropriate contacts between the conducting covers and provide protection for the laser flash instrument. The thus-measured 1D thermal diffusivity can be converted to 1D thermal conductivity after obtaining the specific heat of the sample from differential scanning calorimetry measurements (DSC Q2000, TA Instruments). We also qualitatively observed the microstructure evolution of the GNS/LDH particles during the on/off cycles of the electric field by an inverted microscope (ZEISS AXIO vert.A1) and a high-speed camera (FASTCAM Mini UX 50).

3. Results and discussion

3.1. Theoretical results

To verify the validity of the two-step model, we first compared the theoretical results with experiments of graphite/hexadecane suspensions undergoing liquid-solid phase transitions [9] to test how our model applies to an aggregate system. Graphite flakes are dispersed uniformly in the liquid state above a phase transition temperature, but form aggregates in the solid state [9]. So Nan's model [35] was used to calculate the thermal conductivity of the system in the liquid state, while our two-step model (equation (11)) was used in the solid state. Nan's model predicts the thermal conductivity of the suspension as

$$k_{\mathrm{eff}}^{*} = \frac{3 + \phi[(2(k_p - k_f)/(k_f + L_{11}(k_p - k_f))(1 - L_{11}) + (k_p - k_f)/(k_f + L_{33}(k_p - k_f)(1 - L_{33}))]}{3 - \phi[2(k_p - k_f)/(k_f + L_{11}(k_p - k_f))L_{11} + (k_p - k_f)/(k_f + L_{33}(k_p - k_f))L_{33}]}. \quad (14)$$

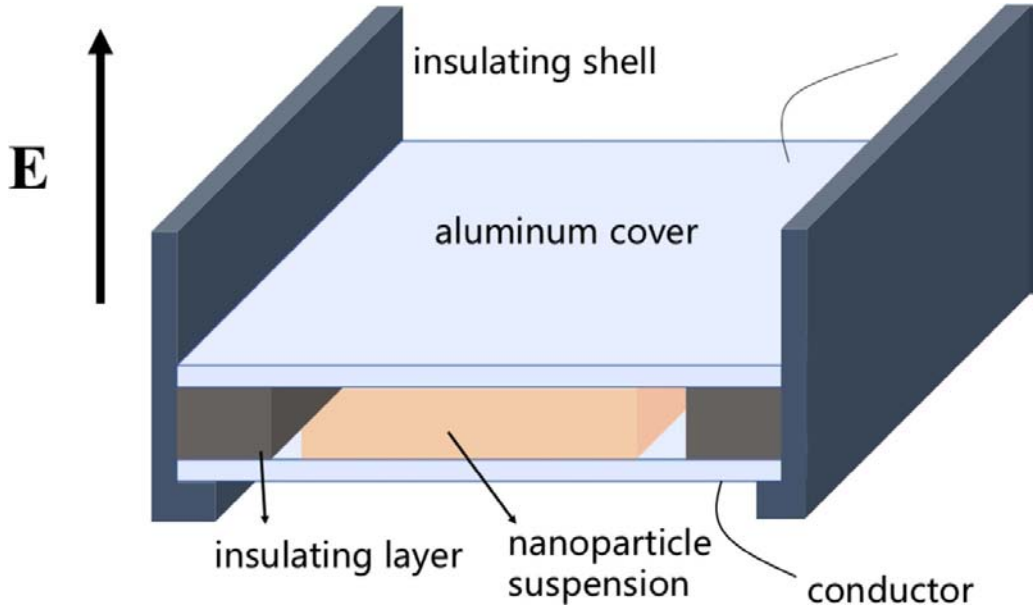

Figure 2. The schematic diagram of self-designed integrated sample cell. The container is composed of aluminum cover, insulating shell and insulating layer. The conductors are adhered onto the aluminum covers to ensure a uniform electrical field. The electric field direction is parallel to the direction of thermal measurement.

Here L_{11}, L_{33} is the geometrical factor depending on the aspect ratio of particle p',

$$L_{11} = L_{22} = \frac{p'^2}{2\left(p'^2 - 1\right)} - \frac{p'}{2\left(p'^2 - 1\right)^{\frac{3}{2}}}\cosh^{-1}p' \quad (15)$$

$$L_{33} = 1 - 2L_{11} \quad (16)$$

The thermal conductivities of the base fluid and graphite flakes were determined from the experimental data in [41] to be $k_f = 0.15\ W/(\mathrm{m}\cdot\mathrm{K})$ and $k_p = 190\ W/(\mathrm{m}\cdot\mathrm{K})$. The aspect ratio of aggregates p and aspect ratio of particles p' was determined roughly from the experimental SEM image in [9] as $p = 500$ and $p' = 30$ and the volume fraction of the nanoparticles in aggregates was obtained by fitting the experimental results, ϕ_{int}=0.68. As shown in figure 3, Nan's model [35] can give accurate predictions when the particles are well dispersed in the liquid state, but becomes inadequate when the particles form aggregates. Instead, our two-step model is more appropriate in the latter case, which shows good fitting to the experiments covering the particle volume fraction ϕ range of $0 \sim 1\%$. The results in figure 3 also clearly show that the form of aggregations can enhance the thermal conductivity of the suspensions significantly.

Next, we turn to test how our two-step model behaves regarding the effect of particle orientation and alignment, and we compared with the experiments in [42]. Maxwell's model is considered accurate for suspensions with low volume fraction and random particle distribution. So k_p was calculated from the experimental data of [42] by Maxwell's model as $k_p = 80\ \mathrm{W/m\cdot K}$. We also substituted $k_f = 0.124\ W/(\mathrm{m}\cdot\mathrm{K})$, aspect ratios $p = 7$, $p = 3$ and $\phi_{int}|_{p=7}$=0.37, $\phi_{int}|_{p=3}$=0.24 (estimated from figure 3 in [42]) into our model, i.e. equation (11). As shown in figure 4, the theoretical results at $<\cos\theta \geq 1$ (indicating perfect alignment) fit with the experimental results relatively well, suggesting that our model is appropriate to predict the thermal conductivities of the system when the particles have large orientational variation. The enhancement ratio between the aligned state ($<\cos\theta \geq 1$) and randomly oriented state ($<\cos\theta \geq 1/3$) could achieve $\sim$1.67$\times$ at $p = 7$, $\phi = 2\%$. It is evident that the orientation of nanoparticles plays a great role on the enhancement of thermal conductivity. These chain-like structures can form effective thermal conductive pathways, thus enhancing the thermal conductivity of the materials along this direction. Further increasing the aspect ratio of the particles up to $p = 20$, we predicted an increasing enhancement ratio theoretically (from $\sim$1.67$\times$ to 2.27$\times$ when p increase from 7 to 20) (figure 4). The results indicate that anisotropic nanoparticles with larger aspect ratio, which could form longer aggregates, are better candidates for thermal conductivity switching in suspensions.

What is the possible maximum thermal switching ratio that could be achieved for these anisotropic-shaped particle suspensions at optimal conditions? We would like to provide a rough prediction by using our two-step model. Graphene flakes are known to be one of the best thermal conductive materials, and we decided to use the parameters of graphene in [41] $k_p = 190\ W/(\mathrm{m}\cdot\mathrm{K})$ and base fluid $k_f = 0.15\ W/(\mathrm{m}\cdot\mathrm{K})$. The theoretical results by using equation (11) are shown in figure 5, and we considered the influence of aspect ratio p, particle volume fraction ϕ, and volume fraction of nanoparticles in aggregates ϕ_{int}. In the selected range of low particle volume fraction of ϕ from 0% to 2%, the thermal switching ratio increases almost linearly, while the increase of

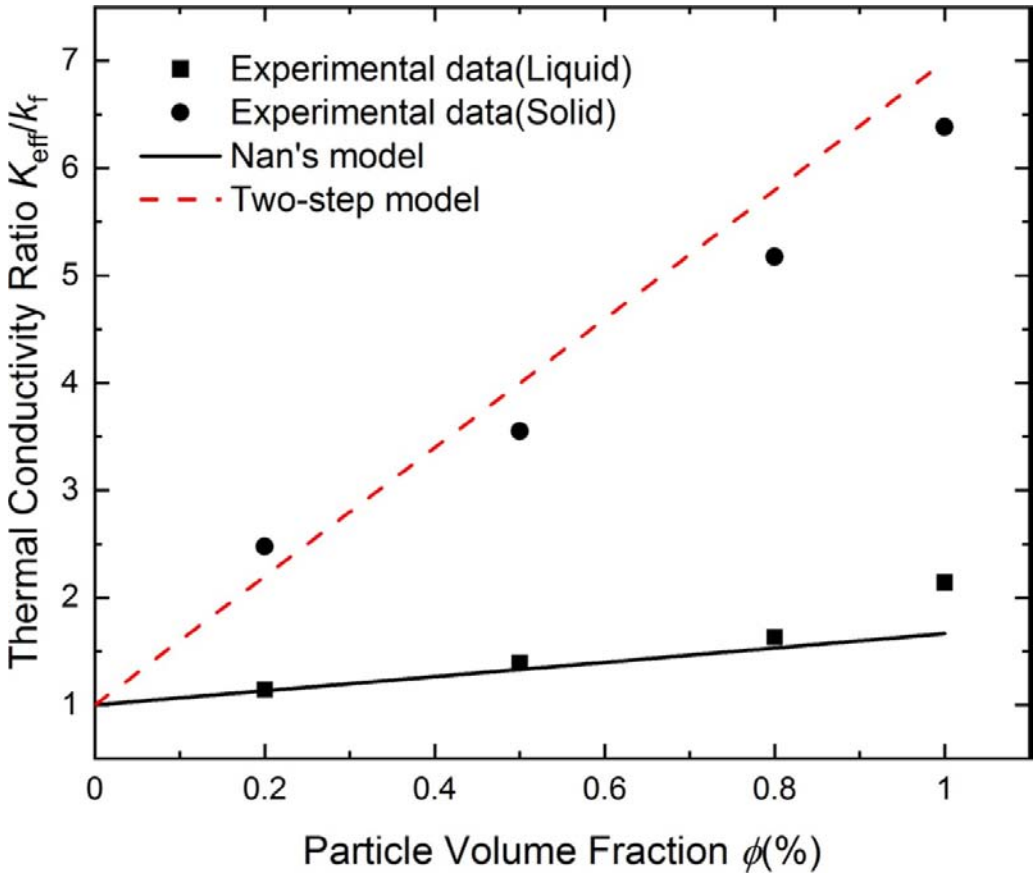

Figure 3. Dependence of the ratio k_{33}/k_f (w-particle/base fluid) on particle volume fraction ϕ. The points are experimental results of graphite/hexadecane suspensions in liquid/solid phase from [9]. The lines are the corresponding theoretical predictions of Nan's model [35] and the two-step model based on the experimental parameters.

ϕ_{int} in the range of $0.2 \sim 0.8$ at constant ϕ ($\phi = \phi_{cluster} \cdot \phi_{int}$, $\phi_{cluster}$ thus decreases) brings the slight decrease. We found that the optimal situation with a maximum thermal switching ratio of $\sim 30\times$ (at $\phi = 2\%$) appears when p is infinite, meaning single chains with infinite length. In fact, when p is over 100, the ratios are close to the above optimal case and changing ϕ_{int} will only affect the results slightly. The above prediction assumes perfect single chains aligned perfectly along one direction, and future experiments are required to check whether this optimal condition can be approached.

3.2. Experimental results

We then set out to experimentally realize the concept of 'thermal smart materials' by selecting proper combination of solid particles and liquid media with tunable structural anisotropy under electric field. GNS are suitable candidates as the dispersive phase in the system due to its high thermal conductivity and large aspect ratio, which are the two good features revealed from the previous theoretical analyses. Unfortunately, pure graphene flakes in itself might not be used directly because the high electrical conductivity may lead to current leaching and power consumption. On the other hand, the layered inorganic materials, such as layered double-hydroxide (LDH) also receive wide investigations due to the anisotropic morphology. The LDH has low enough electrical conductivity to form stable suspensions under electrical field, but its thermal conductivity is relatively low, inadequate for thermal conductivity switching. However, combining the advantages of GNS and LDH, we followed previous studies [37] to synthesize the two-dimensional dielectric nanosheets, GNS/LDH composites, and dispersed them in silicon oil. The GNS/LDH has high shape anisotropy, high thermal conductivity and tunable dynamics and structures under electric field. The composite particle shows a hexagonal plate-like morphology as shown in the SEM image in figure 6(a). GNS grows into small thin-layered patches and attaches to the surface of LDH as shown in figure 6(b), indicating the successful formation of GNS/LDH composites.

We first applied the DC electric field alone at strength of $E = 300$ V mm^{-1}, and recorded the microstructural evolution under an optical microscope, as shown in figure 7. Starting from almost random spatial and orientational distributions in the form of small flocs (figure 7(a)), the particles gradually pack into small ordered chains along the electric field direction (left to right) (figure 7(b)) and finally form long chains with small interchain bridges (figures 7, (c)(d)). The structure remains stable when the field is kept on, but disappears and is replaced by small flocs and broken short chains when the field is turned off (figure 7(e)). Comparing figures 7(e) and (a), we

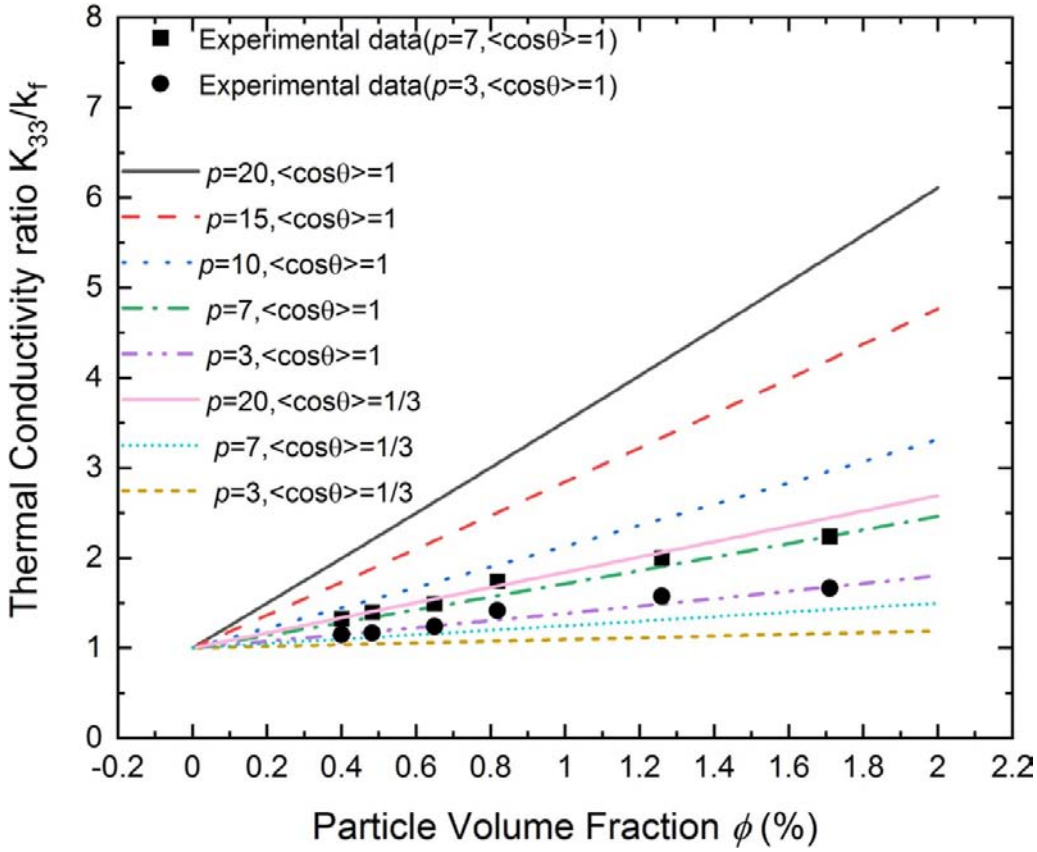

Figure 4. Dependence of the ratio k_{33}/k_f (w-particle/base fluid) on particle volume fraction ϕ. The particle aspect ratio p and orientationl state of the particles ($< \cos\theta \geq 1$, perfectly aligned; $< \cos\theta \geq 1/3$, randomly oriented) are also varied in the plot. The points are experimenal results of $p = 7$ and $p = 3$ in [42] and the lines are predictions from the two-step model.

can see the structure does not completely restore to the initial situation. Some particles tend to stay together due to van der Waals interactions and appear as small separated aggregates after the removal of the external field. Nevertheless, the overall spatial and orientational distributions are randomized after one cycle, showing the partial structural reversibility of the system.

To measure the *in situ* thermal conductivity of the suspension at the presence of electric field, we used the laser flash method (see appendix for details) and held the liquid within the container designed in figure 2. In figure 8(a), we show the thermal conductivity variation with different nanoparticle volume fractions as a function of the electrical field strength E. The thermal conductivity of the suspension increases with E almost linearly, reaches the maximum value at around 700 V mm^{-1}, and then starts to decrease when E further increases. The largest enhancement of thermal conductivity is about 52% (700 V mm^{-1}) with a volume fraction of 15% comparing to the suspension without electric field. An interesting observation here is the non-monotonic dependence of the thermal conductivity k on the field strength E. The initial increase of k arises from the more ordered chains formed at higher E, but the opposite trend after some critical point cannot be explained by this. We suspect as the chain-like structures get thicker in the transverse direction with more sideway branches at higher strength (comparing figure 7(d), 300 V mm^{-1} to figure 7(f), 100 V mm^{-1}), which also results in a decreased aspect ratio, the one-dimensional thermal transport along the lengthwise conductive pathway is hampered. This point can also be drawn from our previous theoretical analyses that the longer single chain with a higher aspect ratio of aggregates can lead to a larger thermal conductivity. The similar rule can explain another observation that the enhancement ratio becomes saturated at high particle volume fraction ϕ as shown in the figure 8(b), while the initial increase with ϕ can be understood from the increased number of conductive pathways. We can conclude here that the optimal enhancement of thermal conductivity occurs at intermediate volume fraction and electric field strength, as large number of well-aligned, long, thin and isolated chains is favored for efficient one-dimensional thermal transport.

Then we tried to compare our experimental results with the two-step model. Here we used $k_f = 0.1\ W/(\mathrm{m}\cdot\mathrm{K})$ as the thermal conductivity of silicone oil, estimated $k_p = 6.5\ W/(\mathrm{m}\cdot\mathrm{K})$ roughly for layered double hydroxide particles by applying the Nan's model to the reported thermal conductivity of LDH nanofluids in [43], and assumed perfect orientation scenario, $< \cos\theta \geq 1$. The aspect ratio p and ϕ_{int} were obtained by quantifying the structures in the microscopic images and fitted from the experimental results, which were summarized in table 1. As shown in figure 9, we could see that the thermal conducvitities of the suspension at low electric

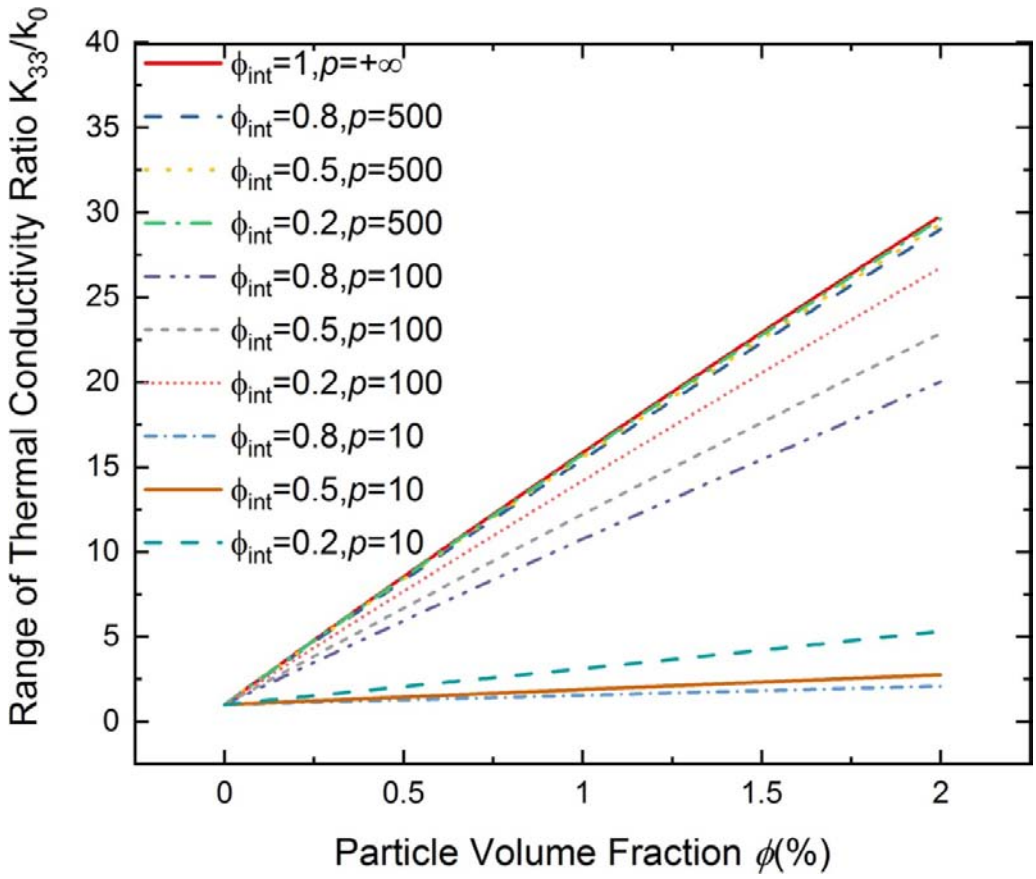

Figure 5. Theoretical predictions of the maximum thermal switching ratio k_{33}/k_0 (aligned/random states) as a function of particle volume fraction ϕ by using the parameters of graphene flakes in [41]. The particle aspect ratio p and volume fraction of nanoparticles in aggregates ϕ_{int} are also varied in the plot.

Table 1. Parameters used in the two-step model to compare with current experimental results of GNS/LDH suspensions.

Electric strength (V mm^{-1})	Aspect ratio p	Volume fraction of particles in aggregates ϕ_{int}
100	1.15	0.97
300	1.70	0.99
700	2.57	0.98
900	1.94	0.98

field strength agree very well with our theoretical model at both low and high particle volume fractions ϕ. However, with the increase of electric strength, the thicker chain-like structures, sideway branches and isolated clusters will become more significant at high ϕ. This still leads to an increase of thermal conductivity ratio k_{33}/k_f (w-particle/base fluid), but less so than linearly, and deviates from that predicted by theory. So the thermal conductivity at high particle volume fraction ϕ is lower than what we expected from the two-step model, as can be seen in figure 9.

When the electric field is turned off, the chain structures are broken into short pieces and redisperse uniformly in the suspension (figure 7(e)). Along with this structural randomization, we found that the thermal conductivity of the system could almost reversibly decrease to the initial value as well, as shown in figure 10. The first on/off cycle shows the largest thermal switching ratio $\sim$1.35×, while the ratios of the following cycles slightly decrease to $\sim$1.28× and become unchanged. The slight irreversibility might originate from the formation of small particle clusters due to particles stuck together (figure 7(e)) after repeated switching on and off the electric field. The situation and the thermal conductivity reversibility might be improved by further functionalization of the particles to make them more stable in the suspension.

4. Conclusions

In this work, we systematically investigated thermal smart materials with reversible thermal conductivities, made of low-dimensional solid particles dispersed in liquid media, by both theoretical and experimental means. Theoretically, we proposed the two-step model, taking into account the particle aggregation and orientational variation simultaneously, and

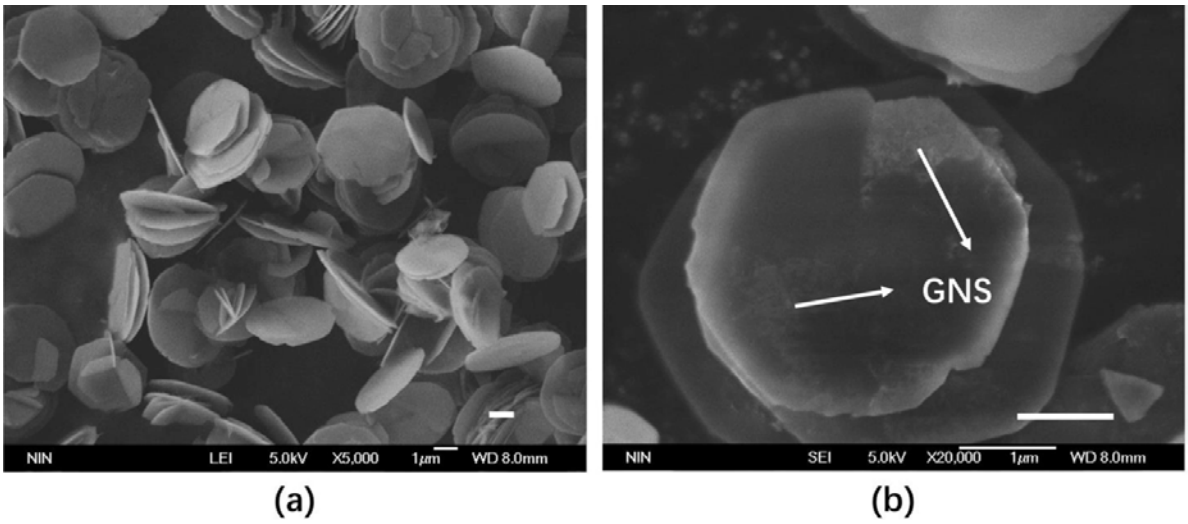

Figure 6. (a) SEM image of GNS/LDH composites and (b) its enlarged view showing the attached GNS. The scale bars in (a) and (b) are 1 μm.

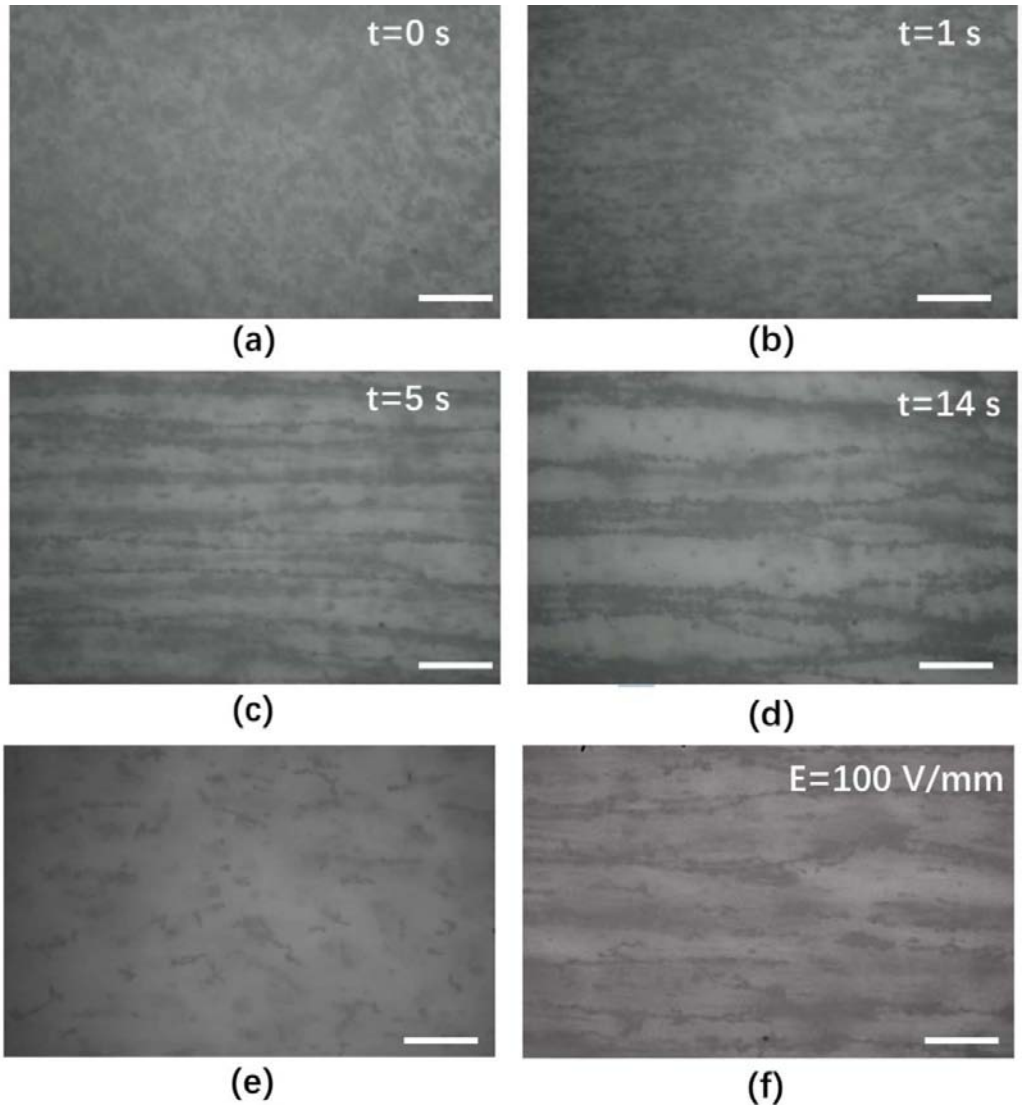

Figure 7. The microstructure evolution of GNS/LDH suspension under DC electrical field. (a) $t = 0$ s, $E = 300$ V mm^{-1}. (b) $t = 1$ s, $E = 300$ V mm^{-1}. (c) $t = 5$ s, $E = 300$ V mm^{-1}. (d) $t = 14$ s, $E = 300$ V mm^{-1}. (e) After the removal of electical field. (f) $t = 14$ s, $E = 100$ V mm^{-1}. The scale bars in (a)–(f) are 200 μm.

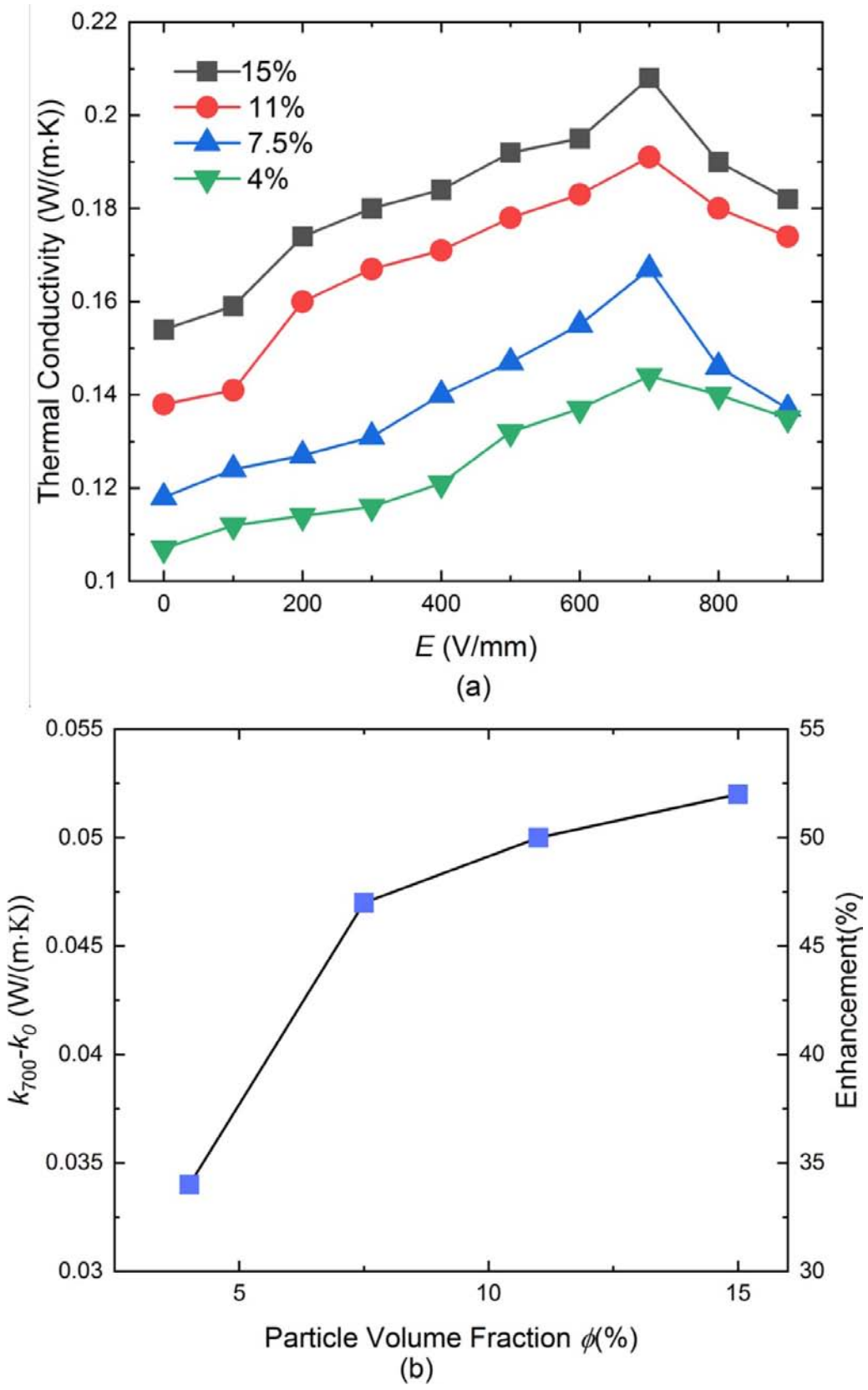

Figure 8. (a) Thermal conductivity variation of GNS-LDH suspensions with different volume fractions as a function of the electrical field strength. (b) Thermal conductivity enhancement of the suspension at $E = 700$ V mm^{-1}.

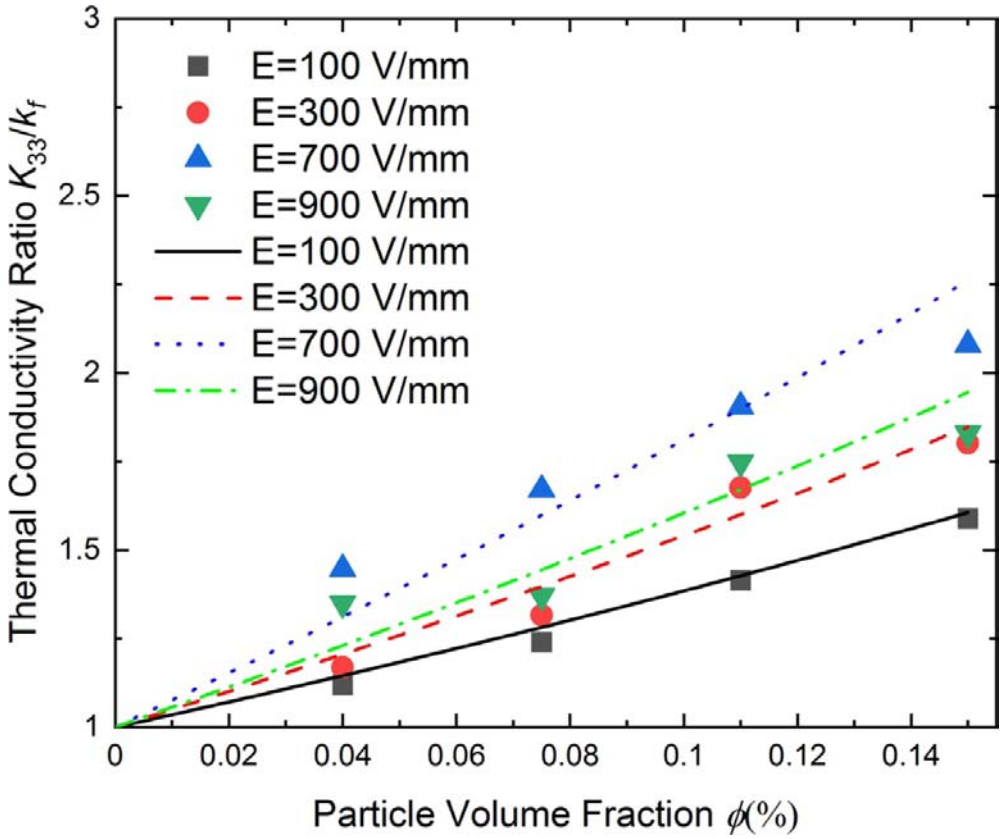

Figure 9. Dependence of the ratio k_{33}/k_f (w-particle/base fluid) on particle volume fraction ϕ. The electrical field strength is also varied in the plot. The soild points are our experimenal results and the lines are predictions from the two-step model.

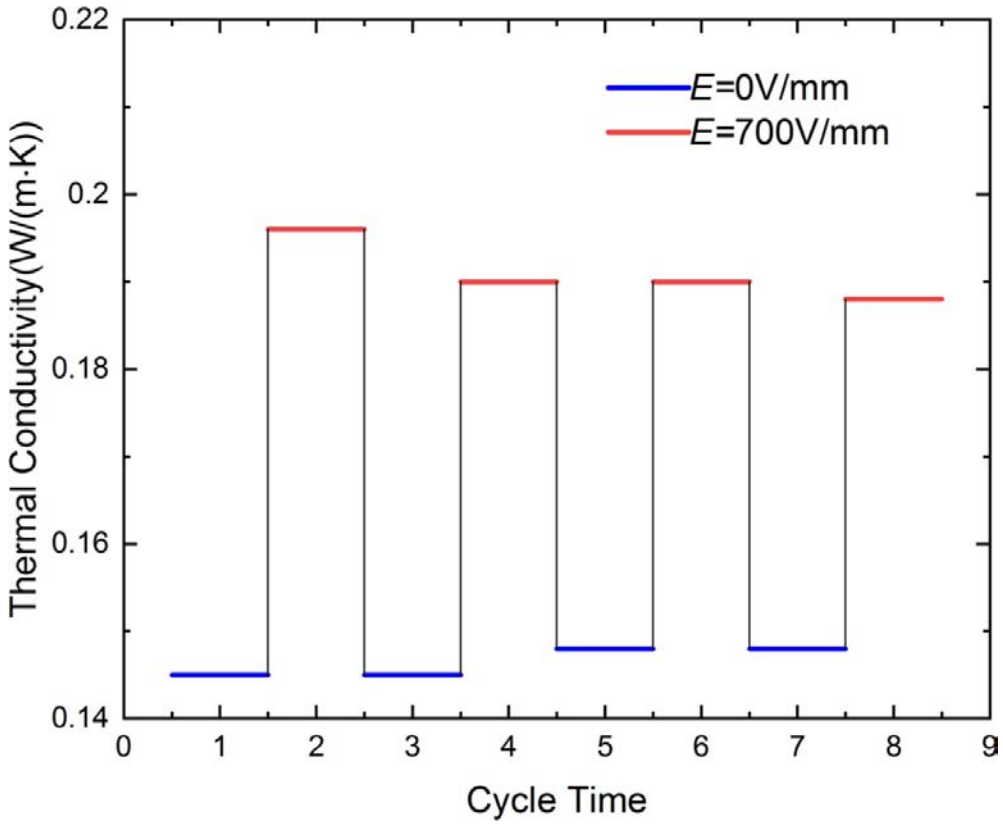

Figure 10. Reversibility testing of thermal conductivity of the GNS-LDH suspension at particle volume fraction of 11% under on/off cycles of DC electric field.

obtained good agreements with experimental results in literature in terms of both the above two effects and with our later experiments as well. We found that the larger aspect ratio of particle aggregates and better alignment could enhance the thermal conductivity of the suspension effectively. The model predicts an unprecedented 30× adjustable range of thermal conductivity, requiring further confirmation by experiments. Experimentally, we prepared GNS/LDH, which have high thermal conductivity due to GNS and good dielectric property due to LDH. Their silicone oil suspensions show elongated chain-like structures under DC electric field. At some optimal volume fraction (15%) and electric field strength (700 V mm^{-1}), the thermal conductivity shows the largest enhancement around 52%. Structural and thermal conductivity reversibility are both observed when the electric field is turned off, and the repeated on/off cycles confirm that the reversibility can be maintained despite small decrease of the switching ratio from ∼1.35× to ∼1.28× at volume fraction of 11%. This work might be a step forward in terms of both the theoretical understanding and preparation techniques for the advancement of thermal smart materials.

Appendix

Laser flash method is a transient technique used to measure the one dimensional thermal diffusivity of materials. It employs a thermal pulse source to one surface of the sample, and monitors the coresponding temperature varation as a function of time on the back surface of the sample with an infrared detector, making the measurement non-contact. The thermal diffusivity along the direction of laser is then calculated.

Assuming the heat transfer process as follows: The sample material is uniform with constant physical properties; the heat conduction is one-dimensional; (2) the thermal pulse is absorbed and converted into heat in a very thin layer on the surface of the sample without heat loss; (3) the pulse time is much shorter than the characteristic time of heat transfer in the sample. The conduction equation is

$$\begin{cases} \frac{\partial^2 T}{\partial x^2} = \frac{1}{\alpha}\frac{\partial T}{\partial t}, (0 < x \langle l, t \rangle 0) \\ -k\frac{\partial T}{\partial x} = Q\delta(t), (x = 0, t > 0) \\ \frac{\partial T}{\partial x} = 0, (x = l, t > 0) \\ T = 0, (0 \le x \le l, t = 0) \end{cases} \tag{A1}$$

Here Q is heat absorption per unit area of the sample, α is the thermal diffusivity, k is thermal conductivity, l is thickness of the sample. The temperature of the back surface is0

$$T(l,t) = T_0 + \frac{Q}{\rho c_p l}\left[1 + 2\sum_1^{\infty}(-1)^n e^{-\frac{n^2\pi^2}{l^2}\alpha t}\right] \tag{A2}$$

When $t \to \infty$, the excess temperature $\theta = T(l,t) - T_0 = \frac{Q}{\rho c_p l}$, reaching maximum value θ_{max}.

$$\theta^*(l,t) = \frac{\theta(l,t)}{\theta_{max}} = 1 + 2\sum_1^{\infty}(-1)^n e^{-\frac{n^2\pi^2}{l^2}\alpha t} \tag{A3}$$

When $\theta^*(l,t) = 0.5$, $\frac{\pi^2 \alpha t}{l^2} = 1.37$. The corresponding time is half time $t_{1/2}$, which can be obtained from temperature curve of back surface.

$$\alpha = 0.1388\frac{l^2}{t_{\frac{1}{2}}} \tag{A4}$$

For liquid thermal smart materials in aluminum sample container, the thermal diffusivity is calculated by the modified 'sandwich' multi-layer model [44]

$$\frac{\partial \ln(\theta\sqrt{t})}{\partial\left(\frac{1}{t}\right)} = \frac{(\chi_1 + \chi_2 + \chi_3)^2}{4} \tag{A5}$$

Here, θ is the dimensionless excess temperature of aluminum cover surface, $\chi_i = \frac{l_i}{\sqrt{\alpha_i}}$, l_i, α_i is the thickness and thermal diffusivity for aluminum cover and liquid, respectively.

Acknowledgments

This work is financially supported by National Natural Science Foundation of China [Nos. 51825601, 51676108].

ORCID iD

Bing-Yang Cao https://orcid.org/0000-0003-3588-972X

References

[1] Moore A L and Shi L 2014 Emerging challenges and materials for thermal management of electronics *Mater. Today* **17** 163–74
[2] Hengeveld D W, Mathison M M, Braun J E, Groll E A and Williams A D 2010 Review of modern spacecraft thermal control technologies *HVAC R Res.* **16** 189–220
[3] Zhu W, Deng Y, Wang Y, Shen S and Gulfam R 2016 High-performance photovoltaic-thermoelectric hybrid power generation system with optimized thermal management *Energy* **100** 91–101
[4] Wehmeyer G, Yabuki T, Monachon C, Wu J and Dames C 2017 Thermal diodes, regulators, and switches: physical mechanisms and potential applications *Appl. Phys. Rev.* **4** 41304
[5] Chang C W, Okawa D, Majumdar A and Zettl A 2006 Solid-state thermal rectifier *Science* **314** 1121–4
[6] Ye Z Q and Cao B Y 2017 Thermal rectification at the bimaterial nanocontact interface *Nanoscale* **9** 11480–7
[7] Sood A *et al* 2018 An electrochemical thermal transistor *Nat. Commun.* **9** 1–9
[8] Li N, Ren J, Wang L, Zhang G, Hänggi P and Li B 2012 Colloquium: phononics: manipulating heat flow with electronic analogs and beyond *Rev. Mod. Phys.* **84** 1045–66
[9] Zheng R, Gao J, Wang J and Chen G 2011 Reversible temperature regulation of electrical and thermal conductivity using liquid-solid phase transitions *Nat. Commun.* **2** 286–9
[10] Shrestha R *et al* 2019 High-contrast and reversible polymer thermal regulator by structural phase transition *Sci. Adv.* **5** eaax3777
[11] Shin J, Kang M, Tsai T, Leal C, Braun P V and Cahill D G 2016 Thermally functional liquid crystal networks by magnetic field driven molecular orientation *ACS Macro Lett* **5** 955–60

[12] Shin J *et al* 2019 Light-triggered thermal conductivity switching in azobenzene polymers *Proc. Natl. Acad. Sci.* **116** 5973–8

[13] Ihlefeld J F, Foley B M, Scrymgeour D A, Michael J R, McKenzie B B, Medlin D L, Wallace M, Trolier-Mckinstry S and Hopkins P E 2015 Room-temperature voltage tunable phonon thermal conductivity via reconfigurable interfaces in ferroelectric thin films *Nano Lett.* **15** 1791–5

[14] Cho J, Losego M D, Zhang H G, Kim H, Zuo J, Petrov I, Cahill D G and Braun P V 2014 Electrochemically tunable thermal conductivity of lithium cobalt oxide *Nat. Commun.* **5** 1–6

[15] Tomko J A, Pena-Francesch A, Jung H, Tyagi M, Allen B D, Demirel M C and Hopkins P E 2018 Tunable thermal transport and reversible thermal conductivity switching in topologically networked bio-inspired materials *Nat. Nanotechnol.* **13** 959–64

[16] Oliva-Avilés A I, Avilés F, Sosa V, Oliva A I and Gamboa F 2012 Dynamics of carbon nanotube alignment by electric fields *Nanotechnology* **23** 465710

[17] Korneva G, Ye H, Gogotsi Y, Halverson D, Friedman G, Bradley J C and Kornev K G 2005 Carbon nanotubes loaded with magnetic particles *Nano Lett.* **5** 879–84

[18] Hobbie E K, Wang H, Kim H, Lin-Gibson S and Grulke E A 2003 Orientation of carbon nanotubes in a sheared polymer melt *Phys. Fluids* **15** 1196–202

[19] Dijkstra D J, Cirstea M and Nakamura N 2010 The orientational behavior of multiwall carbon nanotubes in polycarbonate in simple shear flow *Rheol. Acta* **49** 769–80

[20] Song N, Jiao D, Ding P, Cui S, Tang S and Shi L 2016 Anisotropic thermally conductive flexible films based on nanofibrillated cellulose and aligned graphene nanosheets *J. Mater. Chem.* C **4** 305–14

[21] Marconnet A M, Yamamoto N, Panzer M A, Wardle B L and Goodson K E 2011 Thermal conduction in aligned carbon nanotube-polymer nanocomposites with high packing density *ACS Nano* **5** 4818–25

[22] Cao B-Y and Dong R-Y 2014 Molecular dynamics calculation of rotational diffusion coefficient of a carbon nanotube in fluid *J. Chem. Phys.* **140** 034703

[23] Dong R-Y and Cao B-Y 2015 Anomalous orientations of a rigid carbon nanotube in a sheared fluid *Sci. Rep.* **4** 6120

[24] Dong R Y, Cao P, Cao G X, Hu G J and Cao B Y 2017 DC electric field induced orientation of a graphene in water *Acta Phys. Sin.* **66** 2–9

[25] Monti M, Natali M, Torre L and Kenny J M 2012 The alignment of single walled carbon nanotubes in an epoxy resin by applying a DC electric field *Carbon New York* **50** 2453–64

[26] Hong J Y and Jang J 2012 Highly stable, concentrated dispersions of graphene oxide sheets and their electro-responsive characteristics *Soft Matter* **8** 7348–50

[27] Zhang W L, Liu Y D, Choi H J and Kim S G 2012 Electrorheology of graphene oxide *ACS Appl. Mater. Interfaces* **4** 2267–72

[28] Sun P C, Huang Y, Zheng R T, Cheng G A, Wan Q M and Ding Y L 2015 Magnetic graphite suspensions with reversible thermal conductivity *Mater. Lett.* **149** 92–94

[29] Maxwell J C 1873 A treatise on electricity and magnetism *Nature* vol **7** 478–80

[30] Hamilton R L and Crosser O K 1962 Thermal conductivity of heterogeneous two-component systems *Ind. Eng. Chem. Fundam.* **1** 187–91

[31] Bruggeman D A G 1936 Berechnung verschiedener physikalischer Konstanten von heterogenen Substanzen. II. Dielektrizitätskonstanten und Leitfähigkeiten von Vielkristallen der nichtregulären Systeme *Ann. Phys.* **417** 645–72

[32] Xuan Y and Li Q 2003 Investigation on convective heat transfer and flow features of nanofluids *J. Heat Transfer* **125** 151–5

[33] Yu W and Choi S U S 2004 The role of interfacial layers in the enhanced thermal conductivity of nanofluids: a renovated Hamilton-Crosser model *J. Nanoparticle Res.* **6** 355–61

[34] Prasher R, Evans W, Meakin P, Fish J, Phelan P and Keblinski P 2006 Effect of aggregation on thermal conduction in colloidal nanofluids *Appl. Phys. Lett.* **89** 143119

[35] Nan C W, Birringer R, Clarke D R and Gleiter H 1997 Effective thermal conductivity of particulate composites with interfacial thermal resistance *J. Phys. D: Appl. Phys.* **81** 6692–9

[36] Nan C W 1994 Effective-medium theory of piezoelectric composites *J. Phys. D: Appl. Phys.* **76** 1155–63

[37] Dong Y, Liu Y, Yin J and Zhao X 2014 Preparation and enhanced electro-responsive characteristic of graphene/layered double-hydroxide composite dielectric nanoplates *J. Mater. Chem.* C **2** 10386–94

[38] Marcano D C, Kosynkin D V, Berlin J M, Sinitskii A, Sun Z, Slesarev A, Alemany L B, Lu W and Tour J M 2010 Improved synthesis of graphene oxide *ACS Nano* **4** 4806–14

[39] Marcano D C, Kosynkin D V, Berlin J M, Sinitskii A, Sun Z, Slesarev A S, Alemany L B, Lu W and Tour J M 2018 Correction to Improved Synthesis of Graphene Oxide *ACS Nano* **12** 2078–2078

[40] Sheindlin M, Halton D, Musella M and Ronchi C 1998 Advances in the use of laser-flash techniques for thermal diffusivity measurement *Rev. Sci. Instrum.* **69** 1426–36

[41] Corporation P P and York N 1973 Thermal conductivity of higher saturated n-hydrocarbons over wide ranges of temperature and pressure *J. Eng. Phys.* **24** 465–9

[42] Philip J, Shima P D and Raj B 2007 Enhancement of thermal conductivity in magnetite based nanofluid due to chainlike structures *Appl. Phys. Lett.* **91** 1–4

[43] Chakraborty S, Sarkar I, Haldar K, Pal S K and Chakraborty S 2015 Synthesis of Cu-Al layered double hydroxide nanofluid and characterization of its thermal properties *Appl. Clay Sci.* **107** 98–108

[44] Eriksson R and Seetharaman S 2004 Thermal diffusivity measurements of some synthetic CaO-Al2O3-SiO2 slags *Metall. Mater. Trans.* B **35** 461–9